rspa.royalsocietypublishing.org

Research

Cite this article: Michele S, Sammarco P, d'Errico M. 2016 Theory of the synchronous motion of an array of floating flap gates oscillating wave surge converter. *Proc. R. Soc. A* **472**: 20160174.
http://dx.doi.org/10.1098/rspa.2016.0174

Received: 9 March 2016
Accepted: 1 July 2016

Subject Areas:
ocean engineering, civil engineering, power and energy systems

Keywords:
floating flap gate energy, wave-body interaction, resonance

Author for correspondence:
Simone Michele
e-mail: michele@ing.uniroma2.it

Theory of the synchronous motion of an array of floating flap gates oscillating wave surge converter

Simone Michele, Paolo Sammarco and Michele d'Errico

Department of Civil Engineering and Computer Science, Università degli Studi di Roma 'Tor Vergata', via del Politecnico 1, 00133 Roma, Italy

SM, 0000-0002-4082-6929

We consider a finite array of floating flap gates oscillating wave surge converter (OWSC) in water of constant depth. The diffraction and radiation potentials are solved in terms of elliptical coordinates and Mathieu functions. Generated power and capture width ratio of a single gate excited by incoming waves are given in terms of the radiated wave amplitude in the far field. Similar to the case of axially symmetric absorbers, the maximum power extracted is shown to be directly proportional to the incident wave characteristics: energy flux, angle of incidence and wavelength. Accordingly, the capture width ratio is directly proportional to the wavelength, thus giving a design estimate of the maximum efficiency of the system. We then compare the array and the single gate in terms of energy production. For regular waves, we show that excitation of the out-of-phase natural modes of the array increases the power output, while in the case of random seas we show that the array and the single gate achieve the same efficiency.

1. Introduction

Research on wave energy production by surface-piercing oscillating wave surge converter (OWSCs) has arisen in recent years. This is mainly due to the high performance of these devices in terms of power extraction. Indeed, the floating flap gate OWSC is able to extract energy with large efficiency for a broad range of wave frequencies [1,2]. One disadvantage of such wave energy converter is the large wave load acting at the bottom

THE ROYAL SOCIETY PUBLISHING

foundation in extreme wave conditions. This undesired phenomenon can be reduced dividing the flap into smaller components.

In this paper, we consider an array of neighbouring flap gates in open sea of constant depth under incoming waves. Solutions for the radiation and scattering potentials are found in terms of angular and radial Mathieu functions [3–6]. Application of Mathieu functions in fields such as optics, electromagnetism and ocean surface waves are discussed in [7–10]. Different authors investigated the wave scattering by a stationary platform of elliptical shape partially immersed in the fluid domain [11–13], while Chatjigeorgiou & Mavrakos [14,15] solved the wave diffraction field by arrays of elliptical cylinders. The Mathieu functions have been used also for the solution of the diffraction problem of waves incident on breakwaters of negligible thickness and finite width [16]. To study the mechanical behaviour of the flaps in waves, Renzi & Dias [2] developed a semi-analytical model of the hydrodynamics of a 'thin-flap' by a hypersingular integral equation approach. Michele *et al.* [17,18] have extended the integral approach of Renzi & Dias [2] to multiple array of flaps of finite thickness. However, systematic lengthy numerical investigations are necessary to analyse the parametric dependence of the system response. The present analytical findings allow explicit parametrical insight.

We consider the response of the array to incident waves of varying frequency and angle of incidence. We show that both odd and even natural modes of the array can be excited if the waves are not normally incident to the array [19–22]. The added inertia, radiation damping and exciting torque have explicit expressions. First, the case of a single gate is considered. Useful expressions for the generated power and capture width ratio are derived in terms of the amplitude of the radiated waves in the far field. A closed formula for the maximum power output of a single gate is obtained: the maximum power output is proportional to twice the incident wave power multiplied by the wavelength. Consequently, the capture width ratio is directly proportional to the wavelength. Such a result is of practical interest and could be used in the preliminary design processes to assess the optimal efficiency of the device. The present findings were previously obtained from the analysis of the optimum efficiency of axially symmetric absorbers [23,24]. Indeed, we show that a floating flap gate ('flap' in the following) OWSC achieves the same optimum efficiency of a floating cylinder bottom-hinged OWSC having diameter equal to the flap width. Finally, the array is compared in terms of energy production to the single flap. The analysis in monochromatic waves shows that linear excitation of the natural modes of the array allows maximization of the capture width ratio. In the case of random seas represented by the JONSWAP spectrum [25], the array and the single flap exhibit a similar behaviour in terms of power extraction.

2. Governing equations

With reference to figure 1, consider an array of Q identical flaps in open sea of constant depth h. Let a and $2b$ be, respectively, the width and the thickness of each flap; $w = aQ$ represents the total width of the array. Define a three-dimensional Cartesian coordinate system with the x- and y-axes lying on the mean free surface and the z-axis pointing vertically upward. The x-axis is orthogonal to the array, while the y-axis bisects the array. All the flaps are hinged at the bottom and oscillate about the horizontal common axis lying on $x = 0$, $z = -h$. Monochromatic incident waves of amplitude A, period T and angular frequency $\omega = 2\pi/T$ form an angle ψ with the x-axis. Let G_q denote the qth flap and $\Theta_q(t)$ be the angular displacement of G_q, positive clockwise. Each flap G_q spans a y-width given by

$$y \in [y_q, y_{q+1}], \quad y_q = (q-1)a - \frac{w}{2}, \quad q = 1, \ldots, Q. \tag{2.1}$$

Define $\Theta(y,t)$ as the angular displacement function of the array:

$$\Theta(y,t) = \{\Theta_1(t), \ldots, \Theta_q(t), \ldots, \Theta_Q(t)\}. \tag{2.2}$$

$\Theta(y,t)$ is an unknown piece-wise constant function in $y \in [-w/2, w/2]$.

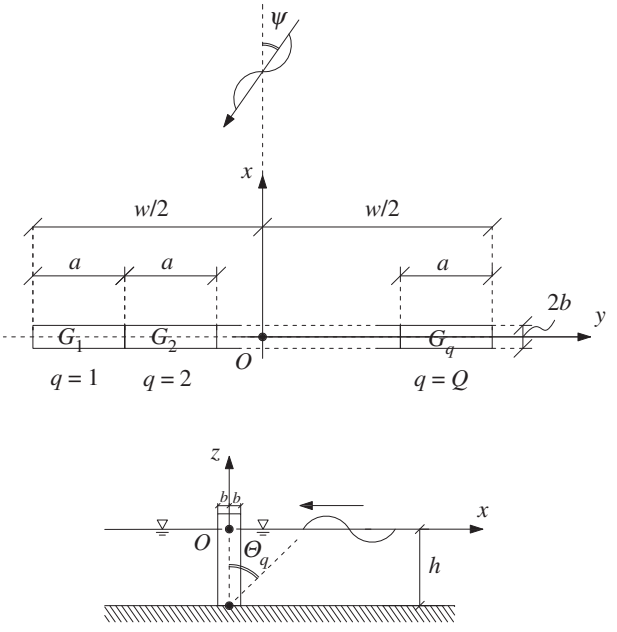

Figure 1. Plan geometry and side view.

We resort to the 'thin-flap' approximation of Martin & Rizzo [26] (see also [2,27]), $b \ll a$, so that $x^{\pm} = \pm 0$ indicates the x-coordinate of the rest position of the vertical surface of the flaps. The horizontal boundary S_q of the flap G_q and the entire horizontal array boundary S_A can then be defined as follows:

$$S_q = \{x = x^{\pm},\ y \in [y_q, y_{q+1}]\} \quad \text{and} \quad S_A = \sum_{q=1}^{Q} S_q. \tag{2.3}$$

The fluid is assumed inviscid and incompressible and the flow irrotational, hence there exist a velocity potential $\Phi(x, y, z, t)$ which satisfies the Laplace equation in the fluid domain Ω:

$$\nabla^2 \Phi = 0, \quad (x, y, z) \in \Omega. \tag{2.4}$$

On the basis of linearized water-wave theory, the potential $\Phi(x, y, z, t)$ satisfies the mixed boundary condition on the free surface

$$\frac{\partial^2 \Phi}{\partial t^2} + g \frac{\partial \Phi}{\partial z} = 0, \quad z = 0, \tag{2.5}$$

and the no-flux condition at the bottom

$$\frac{\partial \Phi}{\partial z} = 0, \quad z = -h. \tag{2.6}$$

For small-amplitude oscillations, the kinematic condition on the surfaces of the array may be written:

$$\frac{\partial \Phi}{\partial x} = \frac{\partial \Theta}{\partial t}(z + h), \quad x, y \in S_A,\ z \in [-h, 0]. \tag{2.7}$$

Assuming harmonic motion of frequency ω, the time dependence can be factored out:

$$\Phi(x, y, z, t) = \mathrm{Re}\{\phi(x, y, z)\, \mathrm{e}^{-\mathrm{i}\omega t}\} \quad \text{and} \quad \Theta(y, t) = \mathrm{Re}\{\theta(y)\, \mathrm{e}^{-\mathrm{i}\omega t}\}, \tag{2.8}$$

where $\theta(y) = \{\theta_1, \ldots, \theta_q, \ldots, \theta_Q\}$ is the displacement amplitude function of the array. The spatial potential $\phi(x, y, z)$ is decomposed into

$$\phi = \phi^{\mathrm{I}} + \phi^{\mathrm{S}} + \sum_{q=1}^{Q} \phi_q^{\mathrm{R}}, \tag{2.9}$$

in which

$$\phi^{\mathrm{I}} = -\frac{\mathrm{i}Ag}{\omega} \frac{\cosh k_0(h+z)}{\cosh k_0 h} \mathrm{e}^{-\mathrm{i}k_0(x\cos\psi + y\sin\psi)}, \tag{2.10}$$

is the potential of the monochromatic incoming waves with incidence angle ψ, ϕ^{S} is the potential of the scattered waves by the array and ϕ_q^{R} is the potential of the radiated waves due to the moving flap G_q while all the other flaps are at rest. In (2.10), k_0 represents the wavenumber, i.e. the real root of the dispersion relation $\omega^2 = gk_0 \tanh k_0 h$ and i is the imaginary unit. Both ϕ_q^{R} and ϕ^{S} satisfy the Laplace equation (2.4), the mixed boundary condition on the free surface (2.5) and the no-flux condition on the seabed (2.6). The kinematic boundary conditions on the array surfaces become

$$\begin{cases} \dfrac{\partial \phi_q^{\mathrm{R}}}{\partial x} = -\mathrm{i}\omega\theta_q(z+h), & x, y \in S_q,\ z \in [-h, 0], \\ 0, & \text{elsewhere on the array} \end{cases} \tag{2.11a}$$

and

$$\frac{\partial \phi^{\mathrm{S}}}{\partial x} = -\frac{\partial \phi^{\mathrm{I}}}{\partial x}, \quad x, y \in S_{\mathrm{A}},\ z \in [-h, 0]. \tag{2.11b}$$

Finally, it is required that ϕ_q^{R} and ϕ^{S} remain bounded for $\sqrt{x^2 + y^2} \to \infty$.

3. Solution for the scattering and radiation problems

Separation of the z-coordinate gives [24]

$$\begin{Bmatrix} \phi_q^{\mathrm{R}} \\ \phi^{\mathrm{S}} \end{Bmatrix} = \sum_{n=0}^{\infty} \begin{Bmatrix} \varphi_{qn}^{\mathrm{R}}(x, y) \\ \varphi_n^{\mathrm{S}}(x, y) \end{Bmatrix} Z_n(z), \tag{3.1}$$

where $Z_n(z)$ are the normalized eigenfunctions:

$$Z_n(z) = \frac{\sqrt{2}\cosh k_n(h+z)}{(h + (g/\omega^2)\sinh^2 k_n h)^{1/2}}, \quad \int_{-h}^{0} Z_n Z_m \,\mathrm{d}z = \delta_{nm}, \quad n, m = 0, 1, \ldots \tag{3.2}$$

and δ_{nm} is the Kronecker symbol. In (3.2), k_n for $n \geq 1$ are the complex roots of the dispersion relation (see again [24])

$$k_n = \mathrm{i}\bar{k}_n, \quad \omega^2 = -g\bar{k}_n \tan \bar{k}_n h, \quad n = 1, \ldots, \infty. \tag{3.3}$$

Following separation of (3.1), the Laplace equation becomes the Helmholtz equation

$$\left(\frac{\partial^2}{\partial x^2} + \frac{\partial^2}{\partial y^2} + k_n^2 \right) \begin{Bmatrix} \varphi_{qn}^{\mathrm{R}}(x, y) \\ \varphi_n^{\mathrm{S}}(x, y) \end{Bmatrix} = 0. \tag{3.4}$$

The boundary conditions on the array (2.11a,b) become, for $q = 1, \ldots, Q$:

$$\begin{cases} \dfrac{\partial \varphi_{qn}^{\mathrm{R}}}{\partial x} = -\mathrm{i}\omega\theta_q f_n, & \text{on } S_q, \\ 0, & \text{elsewhere on the array} \end{cases} \tag{3.5a}$$

and

$$\frac{\partial \varphi_n^{\mathrm{S}}}{\partial x} = Ad_n \cos\psi\, \mathrm{e}^{-\mathrm{i}k_n y \sin\psi}, \quad \text{on } S_{\mathrm{A}}. \tag{3.5b}$$

$\varphi_{qn}^{\mathrm{R}}$ and φ_{n}^{S} must be bounded as $\sqrt{x^2+y^2}\to\infty$. In the latter expressions, the coefficients f_n and d_n are

$$f_n=\int_{-h}^{0}(z+h)Z_n(z)\,\mathrm{d}z=\frac{\sqrt{2}(1-\cosh k_nh+k_nh\,\sinh k_nh)}{(h+(g/\omega^2)\sinh^2 k_nh)^{1/2}k_n^2},\quad n=0,1,\ldots \tag{3.6}$$

and

$$\begin{aligned}d_0&=\int_{-h}^{0}\frac{gk_0Z_0(z)\cosh k_0(h+z)}{\omega\cosh k_0h}\,\mathrm{d}z\\&=\frac{gk_0(h+(g/\omega^2)\sinh^2 k_0h)^{1/2}}{\sqrt{2}\omega\cosh k_0h},\quad d_n=0\quad\text{for } n\geq 1.\end{aligned} \tag{3.7}$$

For the above stated boundary value problems in x,y,z, only semi-analytical solutions are possible. Hence we resort to elliptic coordinates (ξ,η), defined as

$$x=\frac{w}{2}\sinh\xi\sin\eta\quad\text{and}\quad y=\frac{w}{2}\cosh\xi\cos\eta. \tag{3.8}$$

Curves of constant ξ and η describe, respectively, confocal ellipses and hyperbolas of focal length w. The suitability of these coordinates lies in the fact that for $\xi=0$ the ellipse degenerates into a segment of width w described by $\xi=0$ and $\eta\in[0,2\pi]$. Hence, the flap boundary conditions are given on a curve describable by a single coordinate and separation of variables is still possible (Mei [28]). Substitution of (3.8) into (3.4) yields the two-dimensional Helmholtz equation in elliptic coordinates:

$$\left[\frac{\partial^2}{\partial\eta^2}+\frac{\partial^2}{\partial\xi^2}+\frac{w^2k_n^2}{8}(\cosh 2\xi-\cos 2\eta)\right]\begin{Bmatrix}\varphi_{qn}^{\mathrm{R}}(\xi,\eta)\\ \varphi_{n}^{\mathrm{S}}(\xi,\eta)\end{Bmatrix}=0. \tag{3.9}$$

Separation of variables

$$\varphi_{qn}^{\mathrm{R}}(\xi,\eta)=\mathcal{X}_{qn}^{\mathrm{R}}(\xi)\mathcal{Y}_{qn}^{\mathrm{R}}(\eta)\quad\text{and}\quad\varphi_{n}^{\mathrm{S}}(\xi,\eta)=\mathcal{X}_{n}^{\mathrm{S}}(\xi)\mathcal{Y}_{n}^{\mathrm{S}}(\eta), \tag{3.10}$$

and substitution in (3.9) yields the following system of linear ordinary differential equations:

$$\left(\frac{d^2}{\partial\xi^2}-\lambda+2\tau_n\cosh 2\xi\right)\begin{Bmatrix}\mathcal{X}_{qn}^{\mathrm{R}}\\ \mathcal{X}_{n}^{\mathrm{S}}\end{Bmatrix}=0 \tag{3.11}$$

and

$$\left(\frac{d^2}{\partial\eta^2}+\lambda-2\tau_n\cos 2\eta\right)\begin{Bmatrix}\mathcal{Y}_{qn}^{\mathrm{R}}\\ \mathcal{Y}_{n}^{\mathrm{S}}\end{Bmatrix}=0, \tag{3.12}$$

where $\tau_n=w^2k_n^2/16$ is a non-dimensional parameter, while λ is a separation constant. For $n=0$, τ_0 has the physical meaning of the ratio between the array width w and the incident wavelength $2\pi/k_0$. Equations (3.11) and (3.12) are known, respectively, as radial Mathieu equation and angular Mathieu equation [3,5,29]. The radial Mathieu equation plays a similar role as the Bessel equation in cylindrical coordinates and admits solutions expressed in terms of Hankel–Mathieu functions (see appendix A for details). The angular Mathieu equation has four classes of solutions expressed in terms of Fourier series (appendix A). As a result, the most general solution for $\varphi_{qn}^{\mathrm{R}}$ and φ_{n}^{S} bounded for $\xi\to\infty$ is given by

$$\begin{aligned}\begin{Bmatrix}\varphi_{qn}^{\mathrm{R}}(\xi,\eta)\\ \varphi_{n}^{\mathrm{S}}(\xi,\eta)\end{Bmatrix}=\sum_{m=0}^{\infty}\Bigg\{&\begin{bmatrix}\mathcal{A}_{qnm}^{\mathrm{R}}\\ \mathcal{A}_{nm}^{\mathrm{S}}\end{bmatrix}\mathrm{ce}_{2m}(\eta;\tau_n)\mathrm{He}_{2m}^{(1)}(\xi;\tau_n)+\begin{bmatrix}\mathcal{B}_{qnm}^{\mathrm{R}}\\ \mathcal{B}_{nm}^{\mathrm{S}}\end{bmatrix}\mathrm{ce}_{2m+1}(\eta;\tau_n)\mathrm{He}_{2m+1}^{(1)}(\xi;\tau_n)\\&+\begin{bmatrix}\mathcal{C}_{qnm}^{\mathrm{R}}\\ \mathcal{C}_{nm}^{\mathrm{S}}\end{bmatrix}\mathrm{se}_{2m+2}(\eta;\tau_n)\mathrm{Ho}_{2m+2}^{(1)}(\xi;\tau_n)+\begin{bmatrix}\mathcal{D}_{qnm}^{\mathrm{R}}\\ \mathcal{D}_{nm}^{\mathrm{S}}\end{bmatrix}\mathrm{se}_{2m+1}(\eta;\tau_n)\mathrm{Ho}_{2m+1}^{(1)}(\xi;\tau_n)\Bigg\},\end{aligned} \tag{3.13}$$

where $\mathrm{ce}(\eta;\tau_n)$ and $\mathrm{se}(\eta;\tau_n)$ are the even and odd Mathieu functions of the first kind, $\mathrm{He}(\xi;\tau_n)$ and $\mathrm{Ho}(\xi;\tau_n)$ are the even and odd Hankel–Mathieu functions of the first kind, while $\mathcal{A}$, $\mathcal{B}$, $\mathcal{C}$ and $\mathcal{D}$ denote the unknown coefficients which can be obtained applying the boundary conditions

on the array surface. Let us first change all spatial derivatives from rectangular coordinates to elliptical coordinates (ξ, η). By the chain rule of differentiation, the boundary conditions on the array surfaces (3.5*a*,*b*) become, for $q = 1, \ldots, Q$

$$\begin{cases} \dfrac{\partial \varphi_{qn}^{\mathrm{R}}}{\partial \xi} = -\mathrm{i}\omega\theta_q f_n \dfrac{w}{2}\sin\eta, & \text{on } S_q, \\ 0, & \text{elsewhere on the array} \end{cases} \tag{3.14a}$$

and

$$\frac{\partial \varphi_n^{\mathrm{S}}}{\partial \xi} = A d_n \frac{w}{2}\cos\psi \sin\eta\, \mathrm{e}^{-\mathrm{i}k_n (w/2)\cos\eta\sin\psi}, \quad \text{on } S_{\mathrm{A}}, \tag{3.14b}$$

where S_q and S_{A} are now defined in the (ξ, η) frame of reference:

$$\left.\begin{aligned} S_q &= \{\xi = 0,\ \eta \in [\eta_{q+1}; \eta_q] \cup [2\pi - \eta_q; 2\pi - \eta_{q+1}]\} \\ \text{and} \qquad S_{\mathrm{A}} &= \{\xi = 0,\ \eta \in [0; 2\pi]\}, \end{aligned}\right\} \tag{3.15}$$

in which

$$\eta_q = \arccos\left[\frac{2(q-1)}{Q} - 1\right]. \tag{3.16}$$

Application of the boundary conditions (3.14*a*,*b*), while resorting to the orthogonal property of the angular Mathieu functions (A 7), yields the constants in (3.13) of the radiation potential:

$$\mathcal{A}_{qnm}^{\mathrm{R}} = \mathcal{B}_{qnm}^{\mathrm{R}} \equiv 0, \tag{3.17}$$

$$\left.\begin{matrix} \mathcal{C}_{qnm}^{\mathrm{R}} \\ \mathcal{D}_{qnm}^{\mathrm{R}} \end{matrix}\right\} = -\mathrm{i}\omega\theta_q f_n w \int_{S_q} \begin{bmatrix} \mathrm{se}_{2m+2}(\eta; \tau_n) \\ \mathrm{se}_{2m+1}(\eta; \tau_n) \end{bmatrix} \frac{\sin\eta\, \mathrm{d}\eta}{2\pi \mathrm{Ho}_{2m+1\xi}^{(1)}(0; \tau_n)} \tag{3.18}$$

and the constants in (3.13) for the scattering potential:

$$\mathcal{A}_{nm}^{\mathrm{S}} = \mathcal{B}_{nm}^{\mathrm{S}} \equiv 0, \tag{3.19}$$

$$\left.\begin{matrix} \mathcal{C}_{nm}^{\mathrm{S}} \\ \mathcal{D}_{nm}^{\mathrm{S}} \end{matrix}\right\} = w A d_n \cos\psi \int_{S_{\mathrm{A}}} \begin{bmatrix} \mathrm{se}_{2m+2}(\eta; \tau_n) \\ \mathrm{se}_{2m+1}(\eta; \tau_n) \end{bmatrix} \frac{\mathrm{e}^{-\mathrm{i}k_n (w/2)\cos\eta\sin\psi} \sin\eta\, \mathrm{d}\eta}{2\pi \mathrm{Ho}_{2m+1\xi}^{(1)}(0; \tau_n)}, \tag{3.20}$$

where the subscript $(\cdot)_\xi$ denotes the derivative of $(\cdot)$ with respect to the radial coordinate ξ. The solutions for $\varphi_{qn}^{\mathrm{R}}$ and φ_n^{S} of (3.13) become

$$\left.\begin{matrix} \varphi_{qn}^{\mathrm{R}}(\xi, \eta) \\ \varphi_n^{\mathrm{S}}(\xi, \eta) \end{matrix}\right\} = \sum_{m=0}^{\infty} \begin{bmatrix} \mathcal{C}_{qnm}^{\mathrm{R}} \\ \mathcal{C}_{nm}^{\mathrm{S}} \end{bmatrix} \mathrm{se}_{2m+2}(\eta; \tau_n) \mathrm{Ho}_{2m+2}^{(1)}(\xi; \tau_n) + \begin{bmatrix} \mathcal{D}_{qnm}^{\mathrm{R}} \\ \mathcal{D}_{nm}^{\mathrm{S}} \end{bmatrix} \mathrm{se}_{2m+1}(\eta; \tau_n) \mathrm{Ho}_{2m+1}^{(1)}(\xi; \tau_n). \tag{3.21}$$

4. Flap motion

The equation of motion of the qth flap coupled with an energy generator at the hinge is formally equivalent to that of a damped harmonic oscillator:

$$(-\omega^2 I + C - \mathrm{i}\omega\nu_{\mathrm{PTO}})\theta_q - \sum_{p=1}^{Q} (\omega^2 \mu_q^p + \mathrm{i}\omega\nu_q^p)\theta_p = F_q, \quad q = 1, \ldots, Q, \tag{4.1}$$

where I is the moment of inertia of the flap about the hinge, C is the buoyancy restoring torque, ν_{PTO} is the power take-off coefficient,

$$F_q = -\mathrm{i}\omega\rho f_0 \frac{w}{2} \left\{ \int_{2\pi-\eta_q}^{2\pi+\eta_{q+1}} \varphi_0^{\mathrm{S}}(0, \eta) \sin\eta\, \mathrm{d}\eta + \int_{\eta_{q+1}}^{\eta_q} \varphi_0^{\mathrm{S}}(0, \eta) \sin\eta\, \mathrm{d}\eta \right\} \tag{4.2}$$

is the exciting torque due to the diffracted waves, while

$$\mu_q^p = \frac{\rho w}{2\omega} \sum_{n=0}^{\infty} f_n \,\mathrm{Im}\left\{ \int_{2\pi-\eta_q}^{2\pi+\eta_{q+1}} \varphi_{pn}^{\mathrm{R}}(0,\eta)\sin\eta\,\mathrm{d}\eta + \int_{\eta_{q+1}}^{\eta_q} \varphi_{pn}^{\mathrm{R}}(0,\eta)\sin\eta\,\mathrm{d}\eta \right\} \tag{4.3}$$

and

$$\nu_q^p = -\rho f_0 \frac{w}{2} \mathrm{Re}\left\{ \int_{2\pi-\eta_q}^{2\pi+\eta_{q+1}} \varphi_{p0}^{\mathrm{R}}(0,\eta)\sin\eta\,\mathrm{d}\eta + \int_{\eta_{q+1}}^{\eta_q} \varphi_{p0}^{\mathrm{R}}(0,\eta)\sin\eta\,\mathrm{d}\eta \right\} \tag{4.4}$$

represent, respectively, the added inertia and the radiation damping of the flap G_q due to the unit rotation of the flap G_p. Equations (4.1) can be written in matrix form:

$$\left[\left(-\omega^2 I + C - \mathrm{i}\omega\nu_{\mathrm{PTO}}\right)\mathbf{I} - \omega^2\mathbf{M} - \mathrm{i}\omega\mathbf{N}\right]\{\theta\} = \{F\}, \tag{4.5}$$

where $\{\theta\}$ is a column vector of length Q that contains all the angular displacements of the flaps, $\mathbf{I}$ is the identity matrix of size $Q \times Q$, $\mathbf{M}$ and $\mathbf{N}$ are, respectively, the non-symmetrical added inertia matrix and the non-symmetrical radiation damping matrix also of size $Q \times Q$:

$$\mathbf{M} = \begin{bmatrix} \mu_1^1 & \cdots & \mu_1^Q \\ \vdots & \ddots & \vdots \\ \mu_Q^1 & \cdots & \mu_Q^Q \end{bmatrix} \quad \text{and} \quad \mathbf{N} = \begin{bmatrix} \nu_1^1 & \cdots & \nu_1^Q \\ \vdots & \ddots & \vdots \\ \nu_Q^1 & \cdots & \nu_Q^Q \end{bmatrix}, \tag{4.6}$$

while $\{F\}$ is a column vector of size Q which contains the values of the exciting torque on each flap G_q:

$$\{F\} = \{F_1, \ldots, F_q, \ldots, F_Q\}^{\mathrm{T}}. \tag{4.7}$$

Once the θ_q are evaluated, the average power absorbed over a wave period $T = 2\pi/\omega$ by the array in monochromatic incident waves is given by

$$P(\omega) = \frac{1}{T}\int_0^T \nu_{\mathrm{PTO}} \sum_{q=1}^{Q} \left(\frac{\mathrm{d}\Theta_q}{\mathrm{d}t}\right)^2 \mathrm{d}t = \frac{1}{2}\omega^2 \nu_{\mathrm{PTO}} \sum_{q=1}^{Q} |\theta_q|^2. \tag{4.8}$$

To assess the performance of the array, we refer to the capture width ratio C_F defined as the ratio between the power output P and the incident wave energy flux per unit absorber width:

$$C_F(\omega) = \frac{P}{EC_g w}, \tag{4.9}$$

where

$$EC_g = \frac{1}{2}\rho g A^2 \frac{\omega}{2k_0}\left(1 + \frac{2k_0 h}{\sinh 2k_0 h}\right) \tag{4.10}$$

is the rate of energy flux.

5. Results and discussion

(a) The case of a single flap

In this section, the case of a single flap ($Q = 1$) excited by incoming waves having angle of incidence ψ is considered. For ease of representation, we drop reference to $q = Q = 1$.

(i) Solution for the scattering and radiation problems

The solution for the radiation potential (3.21) becomes

$$\varphi_n^{\mathrm{R}}(\xi,\eta) = -\mathrm{i}\omega\theta f_n w \sum_{m=0}^{\infty} \frac{B_1^{(2m+1)} \mathrm{Ho}_{2m+1}^{(1)}(\xi;\tau_n)\sin\eta}{2\mathrm{Ho}_{2m+1\,\xi}^{(1)}(0;\tau_n)}, \tag{5.1}$$

where $B_1^{(2m+1)}$ is the first coefficient of se_{2m+1} (appendix A), while the solution for the scattering potential (3.21) is given by

$$\begin{aligned}\varphi_n^{\mathrm{S}}(\xi,\eta) = Ad_n w\cos\psi \sum_{m=0}^{\infty} \frac{\mathrm{se}_m(\eta;\tau_n)\mathrm{Ho}_m^{(1)}(\xi;\tau_n)}{2\mathrm{Ho}_{m\,\xi}^{(1)}(0;\tau_n)} \\ \times \sum_{j=0}^{\infty} B_j^{(m)} \left[\mathrm{i}^{j-1} J_{j-1}\left(-k_n\frac{w}{2}\sin\psi\right) - \mathrm{i}^{-j-1} J_{-j-1}\left(-k_n\frac{w}{2}\sin\psi\right)\right]\end{aligned} \tag{5.2}$$

in which J_j is the Bessel function of the first kind and order j. In the case of normal incidence ($\psi = 0$), the scattering potential further simplifies:

$$\varphi_n^{\mathrm{S}}(\xi,\eta) = Ad_n w \sum_{m=0}^{\infty} \frac{B_1^{(2m+1)} \mathrm{Ho}_{2m+1}^{(1)}(\xi;\tau_n)\sin\eta}{2\mathrm{Ho}_{2m+1\,\xi}^{(1)}(0;\tau_n)}. \tag{5.3}$$

The behaviour of the potentials (5.1) and (5.3) can be analysed near the endpoints of the flaps $y = \pm w/2$. Inversion of (3.8) for $\xi = 0$ and substitution into (5.1)–(5.3) gives

$$\varphi^{(\mathrm{R,S})} \propto \sin\arccos\frac{2y}{w} = \sqrt{1-\frac{4y^2}{w^2}}, \tag{5.4}$$

Note that due to the range of frequencies of engineering interest $\sin\eta \sim \mathrm{se}_m(\eta;\tau_n)$. i.e. near the endpoints $y = \pm w/2$ the velocity potentials (5.1)–(5.3) have a square-root behaviour [2,27,30] and the velocity has a square-root singularity. With the solution of the radiation potential (5.1), the added inertia and the radiation damping are given by

$$\mu = \rho w^2 \pi \sum_{n=0}^{\infty} f_n^2 \,\mathrm{Im}\left\{\sum_{m=0}^{\infty} \frac{B_1^{(2m+1)^2}\mathrm{No}_{2m+1}(0;\tau_n)}{4\mathrm{Ho}_{2m+1,\xi}^{(1)}(0;\tau_n)}\right\} \tag{5.5}$$

and

$$\nu = -\rho\omega w^2 f_0^2 \pi \,\mathrm{Re}\left\{\sum_{m=0}^{\infty} \frac{B_1^{(2m+1)^2}\mathrm{No}_{2m+1}(0;\tau_0)}{4\mathrm{Ho}_{2m+1,\xi}^{(1)}(0;\tau_0)}\right\}. \tag{5.6}$$

To evaluate the exciting torque F for varying ψ, we make use of the three-dimensional Haskind–Hanaoka relation. First of all, we derive the asymptotic behaviour of the radiation potential in the far field ($\xi \to \infty$) for unit rotational velocity of the flap:

$$\sum_{n=0}^{\infty} \phi_n^{\mathrm{R}} \sim -\frac{\mathrm{i}g\mathcal{A}^{\mathrm{R}}(\eta)}{\omega} \frac{\cosh k_0(h+z)}{\cosh k_0 h} \sqrt{\frac{2}{\pi k_0 r}}\, \mathrm{e}^{\mathrm{i}(k_0 r - \pi/4)}, \tag{5.7}$$

where $r = w\,\mathrm{e}^{\xi}/4$ is the radius expressed in terms of the radial elliptic coordinate ξ, while

$$\mathcal{A}^{\mathrm{R}}(\eta) = -\sum_{m=0}^{\infty} \frac{4\omega B_1^{2m+1} Z_0(0) f_0}{2gk_0 w \mathrm{Ho}_{2m+1\,\xi}^{(1)}(0;\tau_n)} \sin\eta \tag{5.8}$$

represents the angular variation of the radially spreading wave [24]. Let $\eta^{\mathrm{I}} = 3\pi/2 - \psi$ denote the angle of incidence η of the incoming waves. The Haskind–Hanaoka relation gives

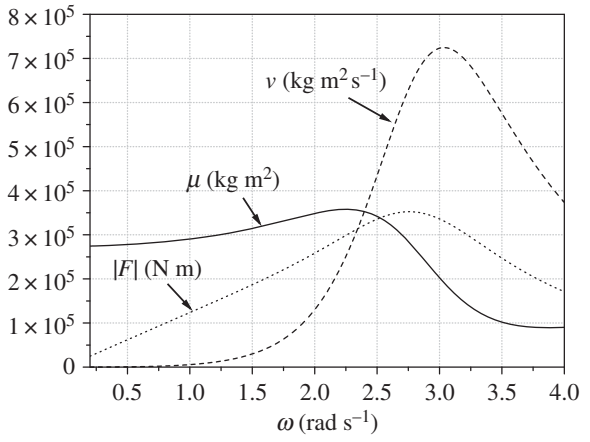

Figure 2. Added inertia μ (continuous line), radiation damping ν (dashed line) and magnitude of the exciting torque $|F|$ (dotted line) versus incident wave frequency ω. The behaviour of these curves is similar to that of [17].

Table 1. Flap and sea depth characteristics. Note that $w = a$ for $Q = 1$. For the case $Q = 5$, $w = 5a$.

parameters	symbol	value
flap width	a	3 m
moment of inertia	I	5×10^4 kg m^2
buoyancy restoring torque	C	7×10^5 Nm
water depth	h	5 m

(see eqn (8.6.41) of [24])

$$F = -\frac{4}{k}\rho g A C_g \mathcal{A}^{\mathrm{R}}(\eta^{\mathrm{I}} + \pi) = -\frac{4}{k}\rho g A C_g \mathcal{A}^{\mathrm{R}}\left(\frac{\pi}{2} - \psi\right)$$
$$= -\frac{4}{k}\rho g A C_g \mathcal{A}^{\mathrm{R}}\left(\frac{\pi}{2}\right)\cos\psi, \tag{5.9}$$

thus, the exciting torque is equal to the exciting torque due to the incoming waves as if they were normally incident on the flap ($\psi = 0$) multiplied by the factor $\cos\psi$. It follows from (5.3) that

$$F = \rho\omega A w^2 f_0 d_0 \pi \cos\psi \sum_{m=0}^{\infty} \frac{B_1^{(2m+1)^2}\mathrm{No}_{2m+1}(0;\tau_0)}{4\mathrm{Ho}^{(1)}_{2m+1,\xi}(0;\tau_0)}. \tag{5.10}$$

The above expression can also be obtained upon direct substitution of (5.2) into (4.2).

The dependence of the added inertia μ, radiation damping ν and magnitude of the exciting torque $|F|$ for $\psi = 0$ on ω is shown in figure 2 for the flap and sea depth characteristics listed in table 1. The curves shown in figure 2 are in perfect agreement with those of Michele *et al.* [17] for a single flap with small finite thickness (see the case for $b = 0.1$ m of [17]) obtained with the semi-analytical hypersingular integral equation approach.

(ii) Wave power extraction

We now turn to the evaluation of the generated power P. Newman [23] has shown that the most general expression of the generated power (see eqn (8.9.26) of [24]) for three-dimensional bodies

in roll motion is

$$P = -\frac{1}{2k_0}\rho g A^2 C_g \left[\frac{2}{\pi}\int_0^{2\pi} |V\mathcal{A}^{\mathrm{R}}(\eta)|^2\,\mathrm{d}\eta + 4\mathrm{Re}\left\{V^*\mathcal{A}^{\mathrm{R}}\left(\frac{\pi}{2}-\psi\right)\right\}\right], \tag{5.11}$$

where C_g is the group velocity, $V = -\mathrm{i}\omega\theta/A$ is the complex angular velocity of the flap per unit incident wave amplitude A and V^* denotes the complex conjugate of V. The maximum value of (5.11) occurs when $\mathrm{d}P/\mathrm{d}V = 0$, i.e. for

$$|V| = \frac{\omega}{A}|\theta| = \frac{\pi|\mathcal{A}^{\mathrm{R}}(\pi/2-\psi)|}{\int_0^{2\pi}|\mathcal{A}^{\mathrm{R}}(\eta)|^2\,\mathrm{d}\eta} \tag{5.12}$$

and is equal to

$$P_{\max} = \frac{2\pi EC_g}{k_0}\frac{|\mathcal{A}^{\mathrm{R}}(\pi/2-\psi)|^2}{\int_0^{2\pi}|\mathcal{A}^{\mathrm{R}}(\eta)|^2\,\mathrm{d}\eta}. \tag{5.13}$$

Consequently, the optimal capture width ratio $C_{F\max}$ from (4.9) is

$$C_{F\max} = \frac{2\pi}{wk_0}\frac{|\mathcal{A}^{\mathrm{R}}(\pi/2-\psi)|^2}{\int_0^{2\pi}|\mathcal{A}^{\mathrm{R}}(\eta)|^2\,\mathrm{d}\eta}. \tag{5.14}$$

For axially symmetric bodies having diameter equal to d, Newman [23] has shown that for normally incident waves

$$P_{\max} = \frac{2EC_g}{k_0} \quad \text{and} \quad C_{F\max} = \frac{2}{dk_0}. \tag{5.15}$$

We now show that the same expressions (5.15) hold for the single flap. Substitution of (5.8) into (5.13) and (5.14) yields

$$P_{\max} = \frac{2EC_g\cos^2\psi}{k_0} \tag{5.16}$$

and

$$C_{F\max} = \frac{2\cos^2\psi}{wk_0}, \tag{5.17}$$

which gives (5.15) for the case $\psi = 0$. Hence a flap gate OWSC has the same optimal efficiency of a bottom-hinged cylindrical OWSC having diameter d equal to w. Note that the maximum generated power does not depend on w and that for a fixed value of the flap width, the lower the wavenumber the larger the optimal efficiency. Expressions (5.16)–(5.17) are of practical engineering interest and can be used as a preliminary design criterion to estimate, respectively, the maximum generated power and the optimal efficiency of a single flap excited by incoming waves having different angles of incidence ψ.

The expression of $P_{\max}$ has been obtained without specifying the PTO-coefficient ν_{PTO}. Given that expression (5.13) must represent the maximum of the power P, whose definition is (4.8), we substitute (5.12) into (4.8) and equate the result to $P_{\max}$ (5.13). This way, we obtain the optimal ν_{PTO} which maximizes the power output:

$$\nu_{\mathrm{PTO}} = \frac{2\rho g C_g}{k_0\pi}\int_0^{2\pi}|\mathcal{A}^{\mathrm{R}}(\eta)|^2\,\mathrm{d}\eta. \tag{5.18}$$

Now, expression (5.18) is in turn equal to the expression of the radiation damping ν in terms of the radiated amplitude in the far field (see eqn (8.6.13) of [24] for roll mode only). Hence, (5.18) is exactly $\nu_{\mathrm{PTO}} = \nu$, which is the condition obtained by maximizing the power output of an absorber tuned to resonance with the frequency of the incoming waves (see eqn (8.9.8) of [24]).

Radiation damping (5.6) and exciting torque (5.10) can be further simplified for small values of $\tau_0 = w^2k_0^2/16$, i.e. if the incident wavelength is larger than the total width of the flap. After some

lengthy but straightforward algebra:

$$\sum_{m=0}^{\infty} \frac{B_1^{(2m+1)^2} \mathrm{No}_{2m+1}(0,\tau_0)}{\mathrm{Ho}^{(1)}_{2m+1,\xi}(0;\tau_0)} \simeq -\frac{1}{\pi\tau_0[1/2+(\mathrm{i}/\pi)(1/\tau_0+\ln\tau_0/4-1/2)]}, \tag{5.19}$$

hence (5.6) and (5.10) become

$$\left.\begin{aligned} F &\simeq -\frac{16\rho\omega A f_0 d_0 \cos\psi}{k_0^2[1/2+(\mathrm{i}/\pi)(1/\tau_0+\ln\tau_0/4-1/2)]} \\ \text{and} \qquad \nu &\simeq \frac{32\rho\omega f_0^2}{k_0^2\{1+[2/\pi(1/\tau_0+\ln\tau_0/4-1/2)]^2\}}. \end{aligned}\right\} \tag{5.20}$$

For given wave frequency ω, expression (4.8) can be maximized if the single flap OWSC is tuned to resonance (i.e. I and C are chosen to satisfy the eigenvalue condition $C-\omega^2(I+\mu)=0$ for given ω) and if ν_{PTO} is equal to the radiation damping ν [24], hence we get

$$P_{\max} = \frac{|F|^2}{8\nu}. \tag{5.21}$$

Substitution of (5.20) in the latter yields:

$$P_{\max} = \frac{2EC_g\cos^2\psi}{k_0}. \tag{5.22}$$

Thus, we obtain again equation (5.16) without recurring to expression (5.8) for the angular variation of the radially spreading wave in the far field $\mathcal{A}^{\mathrm{R}}(\eta)$.

(b) The case of multiple flaps

In this section, the results of the analytical model for a sample case of $Q=5$ flaps are presented and discussed. The values of the parameters which characterize each flap and the sea depth are listed in table 1.

(i) Natural modes and free response

The structure of the angular momentum equation suggests that the array behaves as a linear damped harmonic oscillator. The eigenfrequencies of the system are then evaluated from the solution of the nonlinear eigenvalue condition:

$$\det[(-\omega^2 I + C)\mathbf{I} - \omega^2\mathbf{M}] = 0, \tag{5.23}$$

while the related eigenvectors are evaluated by setting $\theta_1=1$ in the following system:

$$[(-\omega^2 I + C)\mathbf{I} - \omega^2\mathbf{M}]\{\theta\} = 0. \tag{5.24}$$

As in the case of Sammarco *et al.* [19] and Michele *et al.* [17], $(Q-1)$ out-of-phase natural modes and one in-phase mode are obtained in the frequency domain of interest. The numerical values of the eigenfrequencies are listed in table 2. Following the definition of Sammarco *et al.* [19], $N(\omega_1)$, N_1 and N_3 are the even modes. N_2 and N_4 are the odd modes which can be excited only if the direction of the incident waves is not orthogonal to the array surfaces. Solution of the system (4.5) with $\nu_{\mathrm{PTO}}=0$ and $A=1$ m gives the response amplitude operator (RAO) of the array. Two different angles of incidence are considered $\psi=0$ rad and $\psi=\pi/6$ rad. Figure 3 shows the behaviour of the response of each flap G_q for the different values of ψ. Note that in the case of normal incidence (figure 3*a*), $\theta_1=\theta_5$ and $\theta_2=\theta_4$ because of the symmetry of the exciting torque. Indeed, only the even modes are excited ($N(\omega_1)$, N_1 and N_3). On the other hand, if $\psi\neq 0$ also the odd modes can be excited and the peaks related to the excitation of N_2 and N_4 are present (figure 3*b*). Note also that the exciting torque depends on $\cos\psi$ (equation (5.9)), hence the amplitude response of each flap decreases if ψ increases. Moreover, the shape of the array motion

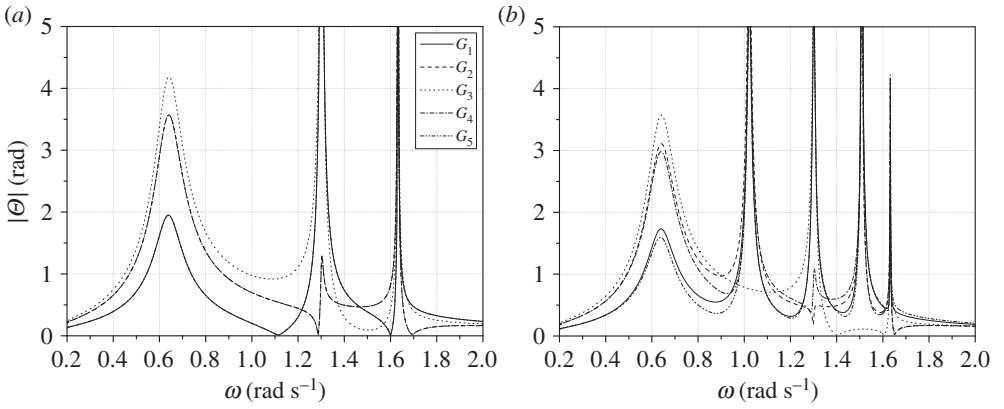

Figure 3. Flap amplitude response versus incident wave frequency for two different values of the angle of incidence ψ. (*a*) $\psi = 0$ rad. (*b*) $\psi = \pi/6$ rad. For $\psi = 0$, only the even modes are excited, conversely, for $\psi \neq 0$, all the out-of-phase natural modes are excited by incoming waves.

Table 2. Eigenfrequencies of the out-of-phase modes and the first in-phase mode.

ω (rad s^{-1})	period (s)	mode
1.63	3.85	N_1
1.51	4.16	N_2
1.34	4.69	N_3
1.02	6.16	N_4
0.66	9.52	$N(\omega_1)$

loses the symmetry with respect to $y = 0$ if $\psi \neq 0$, i.e. $\theta_1 \neq \theta_2 \neq \cdots \neq \theta_5$. This is because both odd and even natural modes are excited.

(ii) Wave power extraction in monochromatic waves

We now compare in terms of power extraction: (i) the array of $Q = 5$ flaps, (ii) a single flap having the same total width of the array, $w = 5a = 15$ m and (iii) a single flap out of the five with $w = a = 3$ m. Consider the first in-phase mode $N(\omega_1)$ of the array and maximize the power output of the three systems when the incident wave frequency is equal to the eigenfrequency of $N(\omega_1)$, i.e. $\omega \equiv \omega_1 = 0.66$ rad s^{-1}. The values of inertia and buoyancy which satisfy the resonance condition for the three systems are listed in table 3. Maximization of the power output gives three corresponding values of ν_{PTO}, also listed in table 3. Figure 4 shows the behaviour of the capture width ratio C_F of each system versus incident wave frequency ω for two different values of the angle ψ. In each of the cases, the maximum is located at $\omega = 0.66$ rad s^{-1} and decreases when ψ increases. Overall, the capture width ratio of the array is larger than that of the other two systems. This is because the out-of-phase modes increase the amplitude response and hence the power output. Note that C_F of the single flap with $w = 3$ m has a narrow peak five times larger than that of the other systems. However, slightly outside $\omega = 0.66$ rad s^{-1}, C_F is almost zero and the flap becomes inefficient. Now consider the expression for $C_{F\max}$ applied to the single flap having $w = 15$ m. Equation (5.17) gives

$$C_{F\max}(\psi = 0) = \frac{2\cos^2 0}{wk_0} \simeq 1.37 \quad \text{and} \quad C_{F\max}\left(\psi = \frac{\pi}{6}\right) = \frac{2\cos^2 \pi/6}{wk_0} \simeq 1.03, \tag{5.25}$$

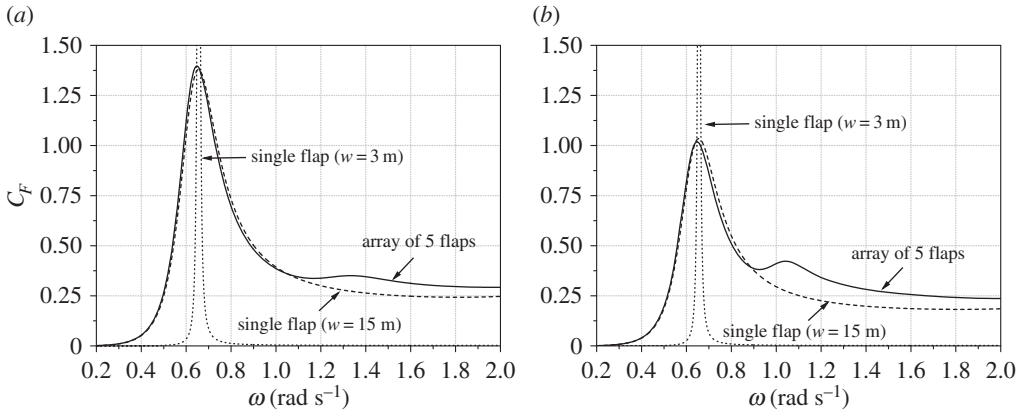

Figure 4. Behaviour of the capture width ratio C_F of each system versus incident wave frequency ω for two different values of the angle of incidence ψ. (*a*) $\psi = 0$ rad. (*b*) $\psi = \pi/6$ rad. In this case, the power take-off coefficient is optimized for the in-phase eigenfrequency ω_1.

Table 3. Total width w, inertia I and buoyancy C of the systems satisfying the resonance condition for $\omega = 0.66$ rad s^{-1} and optimal values of PTO-coefficient ν_{PTO}.

	w (m)	I (kg m^2)	C (N m)	ν_{PTO} (kg m^2 s^{-1})
array of $Q = 5$ flaps	15	5×10^4	7×10^5	2×10^5
single flap	15	25×10^4	35×10^5	10^6
single flap	3	10^4	1.25×10^5	14×10^2

where $k_0 \simeq 0.098\,\mathrm{m}^{-1}$ is the wavenumber related to $\omega = 0.66\,\mathrm{rad\,s}^{-1}$. The numerical values (5.25) are very close to the maximum values shown in figure 4 for the array of Q flaps. This is because the array behaves like a single flap when the in-phase mode is resonated.

The generated power can be maximized also in correspondence to the out-of-phase eigenfrequencies of the array. These modes are nearly trapped and are characterized by the smallness of the radiation damping [17–19]. By choosing $\nu_{PTO} = 10^4\,\mathrm{kg\,m^2\,s^{-1}}$, we obtain the behaviour of C_F shown in figure 5: optimization of the power output is now extended to a broader range of frequencies.

(iii) Wave power extraction in random waves

Now we investigate the behaviour in random waves of the three configurations analysed in the previous section. The JONSWAP spectrum $S_\zeta(\omega)$ has been used to simulate the incident wave field [25]:

$$S_\zeta(\omega) = \frac{\alpha H_s^2}{\omega}\left(\frac{\omega_p}{\omega}\right)^4 \exp\left[-1{,}25\left(\frac{\omega_p}{\omega}\right)^4\right]\gamma^{\exp[-(\omega/\omega_p-1)^2/(2\sigma)]}, \tag{5.26}$$

where

$$\alpha = \frac{0.0624(1.094 - 0.01915\ln\gamma)}{0.23 + 0.0336\gamma - 0.185(1{,}9+\gamma)^{-1}}, \quad \sigma = \begin{cases} 0.07 : \omega \le \omega_p \\ 0.09 : \omega > \omega_p \end{cases}, \quad \gamma = 3.3, \tag{5.27}$$

while H_s and ω_p are, respectively, the significant wave height and the peak frequency. Normal incidence of the incoming waves is assumed, $\psi = 0$. The average absorbed power $\bar{P}$

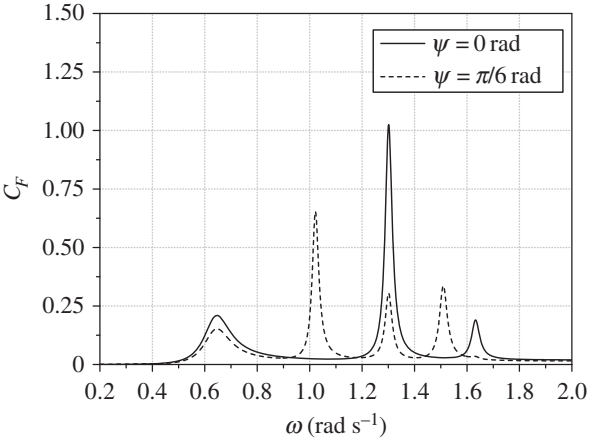

Figure 5. Capture width ratio C_F of the array versus incident wave frequency ω for two different angles of incidence ψ. The PTO-coefficient is optimized for the out-of-phase motion.

can now be defined as [18]:

$$\bar{P} = \nu_{\mathrm{PTO}} \int_0^\infty \sum_{q=1}^{Q} |\theta_q|^2 \omega^2 S_\zeta \, \mathrm{d}\omega, \tag{5.28}$$

where $|\theta_q|$ is the amplitude response of the qth flap for $A = 1$ m. Let P_ζ indicate the total incident wave power per unit crest width:

$$P_\zeta = \int_0^\infty C_g \rho g S_\zeta \, \mathrm{d}\omega, \tag{5.29}$$

the capture width ratio in random seas $C_{F\zeta}$ of the system can then be written as follows:

$$C_{F\zeta} = \frac{\bar{P}}{w P_\zeta}. \tag{5.30}$$

Figure 6*a* shows the behaviour of $C_{F\zeta}$ of each system versus spectral peak frequency ω_{p}. As in previous section, the systems are optimized for the in-phase eigenfrequency $\omega = \omega_1 = 0.66$ rad s^{-1}. The optimal values of ν_{PTO} are those listed in table 3. The maxima of $C_{F\zeta}$ are smaller than the maxima of C_F for regular waves (figure 4*a*). This is because the incident wave spectrum does not couple well with the eigenfrequencies leading to reduction of the efficiency. This occurrence is evident for the case of the single flap having $w = 3$ m. Indeed, the high and narrow peak shown in figure 4*a* decreases from about $C_{F\max} \simeq 6.8$ (accordingly to equation (5.17)) to almost 0.45. Similar phenomena was observed for a different configuration in Michele *et al.* [18]. Consider now the behaviour of $C_{F\zeta}$ for the array and for the single flap having the same width of the array, $w = 15$ m. The array is more efficient than the single flap at the higher peak frequencies. As in monochromatic incident waves, the efficiency benefits of the out-of-phase modes resonance.

First Renzi & Dias [2] and then Michele *et al.* [17,18] showed that the diffraction wave field dominates the dynamics and the efficiency of the system for large values of the PTO-coefficient. In this case, the behaviour of the capture width ratio becomes similar to that of the exciting torque. Figure 6*b* shows the behaviour of $C_{F\zeta}$ of the previous systems but for ν_{PTO} values five times larger than those listed in table 3. The maxima of each curve decrease slightly with respect to the maxima of figure 6*a*. On the other hand, the global efficiency of each system increases, as can be seen by comparing figure 6*a* with figure 6*b* for $\omega_{\mathrm{p}} > 0.8$ rad s^{-1}. Figure 6*b* also shows that the behaviour of $C_{F\zeta}$ for the array and the single flap having $w = 15$ m is very similar for a wide range of peak frequencies. In other words, the benefit of the array out-of-phase modes fades and both systems are equivalent in terms of power extraction and efficiency. Figure 7 shows $C_{F\zeta}$ of the array optimized for the out-of-phase eigenfrequencies versus ω_{p}. The PTO-coefficient is now

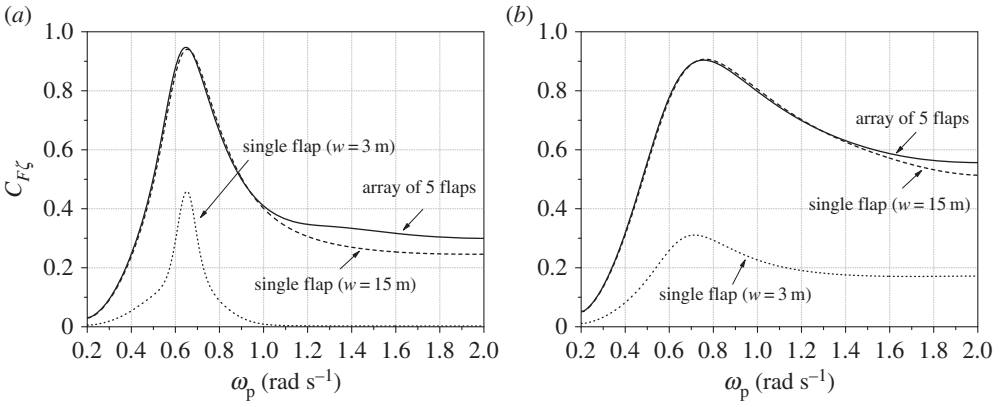

Figure 6. Behaviour of the capture width ratio in random seas $C_{F\zeta}$ of each system versus peak frequency ω_p for different values of ν_{PTO}. (*a*) ν_{PTO} optimized for the in-phase eigenfrequencies (see table 3 for the values). (*b*) ν_{PTO} values five times larger than those listed in table 3. Each system is optimized for the diffraction wave field.

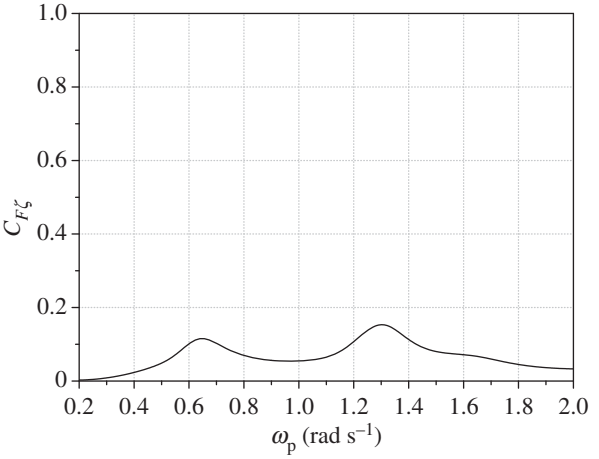

Figure 7. Behaviour of the capture width ratio in random seas $C_{F\zeta}$ of the array versus peak frequency ω_p. The PTO-coefficient $\nu_{PTO} = 10^4$ kg m^2 s^{-1} is optimized for the out-of-phase eigenfrequencies.

$\nu_{PTO} = 10^4$ kg m^2 s^{-1}. In this case, $C_{F\zeta}$ is lower than the counterpart C_F for monochromatic waves (figure 5): the narrower the resonant peak in monochromatic waves the larger the difference between $C_{F\zeta}$ and C_F. We conclude that in random waves is convenient to choose large values of ν_{PTO} in order to increase the bandwidth of $C_{F\zeta}$.

6. Conclusion

We analysed the mechanical behaviour of an array of neighbouring flaps OWSC in open sea. The analytical solution for the radiation and diffraction problems is obtained in terms of Mathieu functions. The explicit analytical expressions of the added inertia, radiation damping and exciting torque are derived and compared with those obtained via the hypersingular integral equation approach, showing excellent agreement between the two models.

Useful parametric expressions for the power output and capture width ratio of a single flap are given in terms of the radiated wave in the far field. Specifically, the maximum power output

is shown to be proportional to twice the rate of energy flux multiplied by the wavelength and the optimal capture width ratio directly proportional to the wavelength. The same results were obtained for axially symmetric absorbers, thus proving that a floating flap gate OWSC is as efficient as a floating cylindrical bottom-hinged OWSC.

Solution of the eigenvalue condition for the array of Q flaps gives $(Q-1)$ out-of-phase natural modes and infinite in-phase modes. Different angles of incidence of the incoming waves are considered. In the case of normal incidence, only the even modes can be resonated. Conversely, if the direction is not normal the odd modes are also resonated and the dynamics of the flaps becomes more articulated. Differently from the case of one flap in open sea, the output power of the array can also be maximized in correspondence of the out-of-phase eigenfrequencies. In regular waves, the array is more efficient than a single flap for a broader range of frequencies. For random waves represented by the JONSWAP spectrum, the maxima of the capture width ratio are smaller than the maxima of the capture width ratio in monochromatic waves. In this last case, the array and the single flap are equivalent in terms of power extraction and efficiency.

The analysis is performed in the framework of ideal fluid, irrotational flow and small amplitude oscillations. Fluid viscosity and vortex shedding should be considered to evaluate dissipative phenomena that may modify the behaviour of the device. For this reason, the development of a nonlinear theory which takes into account all these effects is necessary. This will also allow the evaluation of the flap response when the natural modes are excited through a nonlinear mechanism.

Authors' contributions. All authors participated to the development of the study and to draft the manuscript. All authors gave final approval for publication.

Competing interests. We have no competing interests.

Funding. This research received no specific grant from any funding agency, commercial or not-for-profit sectors.

Acknowledgements. The authors thank the anonymous reviewers for their helpful and constructive comments.

Appendix A

(a) Solution of the angular Mathieu equation

The angular Mathieu equation (3.12) has four classes of periodic solutions with period π or 2π which can be expressed in terms of Fourier series:

$$\left.\begin{matrix}\mathcal{Y}^{\mathrm{R}}_{qn}\\ \mathcal{Y}^{\mathrm{S}}_{n}\end{matrix}\right\} = \begin{cases}\text{Class I} = \displaystyle\sum_{j=0}^{\infty} A_{2j}\cos 2j\eta\\ \text{Class II} = \displaystyle\sum_{j=0}^{\infty} A_{2j+1}\cos(2j+1)\eta\end{cases},$$
$$\left.\begin{matrix}\mathcal{Y}^{\mathrm{R}}_{qn}\\ \mathcal{Y}^{\mathrm{S}}_{n}\end{matrix}\right\} = \begin{cases}\text{Class III} = \displaystyle\sum_{j=0}^{\infty} B_{2j+2}\sin(2j+2)\eta\\ \text{Class IV} = \displaystyle\sum_{j=0}^{\infty} B_{2j+1}\sin(2j+1)\eta\end{cases}, \tag{A 1}$$

where A_{2j}, A_{2j+1}, B_{2j+2} and B_{2j+1} are coefficients depending on τ_n and the separation constant λ. Substitution of (A 1) into the angular Mathieu equation (3.12) yields the following recurrence relation for Class I:

$$\left.\begin{aligned}&\lambda A_0 - \tau_n A_2 = 0,\\ &(\lambda-4)A_2 - \tau_n(2A_0 + A_4) = 0,\\ \text{and}\quad &(\lambda - 4j^2)A_{2j} - \tau_n(A_{2j-2} + A_{2j+2}) = 0, \quad j = 2,3,\ldots,\end{aligned}\right\} \tag{A 2}$$

for Class II:

$$\left.\begin{aligned} &(\lambda-1)A_1-\tau_n(A_1+A_3)=0,\\ \text{and}\quad &(\lambda-4j^2-4j-1)A_{2j+1}-\tau_n(A_{2j-1}+A_{2j+3})=0,\quad j=1,2,\ldots,\end{aligned}\right\} \tag{A 3}$$

for Class III:

$$\left.\begin{aligned} &(\lambda-4)B_2-\tau_nB_4=0,\\ \text{and}\quad &(\lambda-4j^2)B_{2j}-\tau_n(B_{2j-2}+B_{2j+2})=0,\quad j=2,3,\ldots,\end{aligned}\right\} \tag{A 4}$$

and for Class IV:

$$\left.\begin{aligned} &(\lambda-1)B_1-\tau_n(B_3-B_1)=0,\\ \text{and}\quad &(\lambda-4j^2-4j-1)B_{2j+1}-\tau_n(B_{2j-1}+B_{2j+3})=0,\quad j=1,2,\ldots.\end{aligned}\right\} \tag{A 5}$$

The recurrence relations (A 2)–(A 5) are homogeneous systems in the coefficients $A_0, A_1, \ldots$ and $B_1, B_2, \ldots$. Once the eigenvalues (characteristic values) $\lambda=\lambda_m$, $m=0,1,\ldots$ of each linear system are calculated, the corresponding non-trivial solutions of (A 1) are found [3,5,29]:

$$\left.\begin{matrix}\mathcal{Y}^{\mathrm{R}}_{qn}\\ \mathcal{Y}^{\mathrm{S}}_{n}\end{matrix}\right\}=\begin{cases}\text{Class I}=\displaystyle\sum_{m=0}^{\infty}\mathrm{ce}_{2m}(\eta;\tau_n)=\sum_{m=0}^{\infty}\sum_{j=0}^{\infty}A_{2j}^{(2m)}(\tau_n)\cos 2j\eta,\\ \text{Class II}=\displaystyle\sum_{m=0}^{\infty}\mathrm{ce}_{2m+1}(\eta;\tau_n)=\sum_{m=0}^{\infty}\sum_{j=0}^{\infty}A_{2j+1}^{(2m+1)}(\tau_n)\cos(2j+1)\eta,\\ \text{Class III}=\displaystyle\sum_{m=0}^{\infty}\mathrm{se}_{2m+2}(\eta;\tau_n)=\sum_{m=0}^{\infty}\sum_{j=0}^{\infty}B_{2j+2}^{(2m+2)}(\tau_n)\sin(2j+2)\eta,\\ \text{Class IV}=\displaystyle\sum_{m=0}^{\infty}\mathrm{se}_{2m+1}(\eta;\tau_n)=\sum_{m=0}^{\infty}\sum_{j=0}^{\infty}B_{2j+1}^{(2m+1)}(\tau_n)\sin(2j+1)\eta,\end{cases} \tag{A 6}$$

where ce_{2m} and ce_{2m+1} represent the even Mathieu functions of the first kind, respectively, of order $2m$ and $2m+1$, while se_{2m+2} and se_{2m+1} represent the odd Mathieu functions of the first kind, respectively, of order $2m+2$ and $2m+1$. Since the Mathieu functions satisfy the orthogonality condition (see again [5])

$$\int_0^{2\pi}\mathrm{ce}_m\mathrm{ce}_p\,\mathrm{d}\eta=\int_0^{2\pi}\mathrm{se}_m\mathrm{se}_p\,\mathrm{d}\eta=\pi\delta_{mp}, \tag{A 7}$$

after substitution of (A 6) in (A 7), the normalization relations for the Fourier coefficients can be written as

$$2A_0^{(2m)^2}+\sum_{j=1}^{\infty}A_{2j}^{(2m)^2}=\sum_{j=0}^{\infty}A_{2j+1}^{(2m+1)^2}=\sum_{j=0}^{\infty}B_{2j+2}^{(2m+2)^2}=\sum_{j=0}^{\infty}B_{2j+1}^{(2m+1)^2}=1. \tag{A 8}$$

Relations (A 8) are used to evaluate the first coefficients of the recurrence relations $A_0^{(2m)}$, $A_1^{(2m+1)}$, $B_2^{(2m+2)}$ and $B_1^{(2m+1)}$ as follows:

(i) give an initial value for $A_0^{(2m)}$, $A_1^{(2m+1)}$, $B_2^{(2m+2)}$ and $B_1^{(2m+1)}$;
(ii) solve the recurrence relations to evaluate the other coefficients;
(iii) rescale all the coefficients to satisfy normalizations (A 8).

(b) Solution of the radial Mathieu equation

The radial Mathieu equation (3.11) admits solutions expressed in terms of Hankel–Mathieu functions of the first and second kind [5]. Recalling that the waves must be outgoing at large

distances from the array, only the Hankel–Mathieu functions of the first kind are taken into account

$$\left.\begin{matrix}\mathcal{X}_{qn}^{\mathrm{R}}\\ \mathcal{X}_{n}^{\mathrm{S}}\end{matrix}\right\}=\begin{cases}\displaystyle\sum_{m=0}^{\infty}\mathrm{He}_{2m}^{(1)}(\xi;\tau_n)=\sum_{m=0}^{\infty}\mathrm{Je}_{2m}(\xi;\tau_n)+\mathrm{iNe}_{2m}(\xi;\tau_n),\\ \displaystyle\sum_{m=0}^{\infty}\mathrm{He}_{2m+1}^{(1)}(\xi;\tau_n)=\sum_{m=0}^{\infty}\mathrm{Je}_{2m+1}(\xi;\tau_n)+\mathrm{iNe}_{2m+1}(\xi;\tau_n),\\ \displaystyle\sum_{m=0}^{\infty}\mathrm{Ho}_{2m+2}^{(1)}(\xi;\tau_n)=\sum_{m=0}^{\infty}\mathrm{Jo}_{2m+2}(\xi;\tau_n)+\mathrm{iNo}_{2m+2}(\xi;\tau_n),\\ \displaystyle\sum_{m=0}^{\infty}\mathrm{Ho}_{2m+1}^{(1)}(\xi;\tau_n)=\sum_{m=0}^{\infty}\mathrm{Jo}_{2m+1}(\xi;\tau_n)+\mathrm{iNo}_{2m+1}(\xi;\tau_n),\end{cases}\tag{A 9}$$

where Je and Jo are called, respectively, even and odd radial Mathieu functions of the first kind, while Ne and No are called, respectively, even and odd radial Mathieu functions of the second kind. The expressions of Je, Jo, Ne and No can be written in terms of summations of Bessel functions [5,29,31]:

$$\mathrm{Je}_{2m}(\xi;\tau_n)=\frac{\mathrm{ce}_{2m}(0;\tau_n)}{A_0^{(2m)}(\tau_n)}\sum_{j=0}^{\infty}A_{2j}^{(2m)}(\tau_n)J_{2j}(u),\tag{A 10}$$

$$\mathrm{Je}_{2m+1}(\xi;\tau_n)=-\frac{p_{2m+1}}{\sqrt{\tau_n}A_1^{(2m+1)^2}(\tau_n)}\sum_{j=0}^{\infty}(-1)^jA_{2j+1}^{(2m+1)}(\tau_n)[J_j(v_1)J_{j+1}(v_2)+J_{j+1}(v_1)J_j(v_2)],\tag{A 11}$$

$$\mathrm{Jo}_{2m+2}(\xi;\tau_n)=-\frac{s_{2m+2}}{\tau_nB_2^{(2m+2)}(\tau_n)}\sum_{j=0}^{\infty}(-1)^jB_{2j+2}^{(2m+2)}(\tau_n)[J_j(v_1)J_{j+2}(v_2)-J_{j+2}(v_1)J_j(v_2)],\tag{A 12}$$

$$\mathrm{Jo}_{2m+1}(\xi;\tau_n)=\frac{s_{2m+1}}{\sqrt{\tau_n}B_1^{(2m+1)}(\tau_n)}\sum_{j=0}^{\infty}(-1)^jB_{2j+1}^{(2m+1)}(\tau_n)[J_j(v_1)J_{j+1}(v_2)-J_{j+1}(v_1)J_j(v_2)],\tag{A 13}$$

$$\mathrm{Ne}_{2m}(\xi;\tau_n)=\frac{\mathrm{ce}_{2m}(0;\tau_n)}{A_0^{(2m)}(\tau_n)}\sum_{j=0}^{\infty}A_{2j}^{(2m)}(\tau_n)N_{2j}(u),\tag{A 14}$$

$$\mathrm{Ne}_{2m+1}(\xi;\tau_n)=-\frac{p_{2m+1}}{\sqrt{\tau_n}A_1^{(2m+1)^2}(\tau_n)}\sum_{j=0}^{\infty}(-1)^jA_{2j+1}^{(2m+1)}(\tau_n)[J_j(v_1)N_{j+1}(v_2)+J_{j+1}(v_1)N_j(v_2)],\tag{A 15}$$

$$\mathrm{No}_{2m+2}(\xi;\tau_n)=-\frac{s_{2m+2}}{\tau_nB_2^{(2m+2)}(\tau_n)}\sum_{j=0}^{\infty}(-1)^jB_{2j+2}^{(2m+2)}(\tau_n)[J_j(v_1)N_{j+2}(v_2)-J_{j+2}(v_1)N_j(v_2)]\tag{A 16}$$

and

$$\mathrm{No}_{2m+1}(\xi;\tau_n)=\frac{s_{2m+1}}{\sqrt{\tau_n}B_1^{(2m+1)}(\tau_n)}\sum_{j=0}^{\infty}(-1)^jB_{2j+1}^{(2m+1)}(\tau_n)[J_j(v_1)N_{j+1}(v_2)-J_{j+1}(v_1)N_j(v_2)],\tag{A 17}$$

where

$$v_1=\sqrt{\tau_n}\,\mathrm{e}^{-\xi},\quad v_2=\sqrt{\tau_n}\,\mathrm{e}^{\xi},\quad u=v_2-v_1=2\sqrt{\tau_n}\sinh\xi,\tag{A 18}$$

$$p_{2m+1}=\mathrm{ce}_{2m+1}(0;\tau_n)\,\mathrm{ce}'_{2m+1}\left(\frac{\pi}{2};\tau_n\right),\quad s_{2m+1}=\mathrm{se}_{2m+1}\left(\frac{\pi}{2};\tau_n\right)\mathrm{se}'_{2m+1}(0;\tau_n)\tag{A 19}$$

and

$$s_{2m+2}=\mathrm{se}'_{2m+2}\left(\frac{\pi}{2};\tau_n\right)\mathrm{se}'_{2m+2}(0;\tau_n).\tag{A 20}$$

In the latter, the prime in ce′ and se′ denotes the derivative of ce and se with respect to η, while N_j is the Bessel function of the second kind and order j.

References

1. Babarit A, Hals J, Muliawan MJ, Kurniawan A, Moan T, Krokstad J. 2012 Numerical benchmarking study of a selection of wave energy converters. *Renew. Energy* **41**, 44–63. (doi:10.1016/j.renene.2011.10.002)
2. Renzi E, Dias F. 2013 Hydrodynamics of the oscillating wave surge converter in the open ocean. *Eur. J. Mech. B/Fluids* **41**, 1–10. (doi:10.1016/j.euromechflu.2013.01.007)
3. Morse PM, Feshbach H. 1981 *Methods of theoretical physics, parts I and II*. Minneapolis, MN: Feshbach Publishing.
4. Morse PM, Rubenstein PJ. 1938 The diffraction of waves by ribbons and by slits. *Phys. Rev.* **54**, 895–898. (doi:10.1103/PhysRev.54.895)
5. McLachan NW. 1951 *Theory and applications of Mathieu functions*. London, UK: Oxford Press.
6. Stamnes JJ, Spjelkavik B. 1995 New method for computing eigenfunctions (Mathieu functions) for scattering by elliptical cylinders. *Pure Appl. Opt.* **4**, 251–262. (doi:10.1088/0963-9659/4/3/011)
7. Gutiérrez-Vega JC, Rodriguez-Dagnino RM, Meneses-Nava MA, Chavéz-Cerda S. 2003 Mathieu functions, a visual approach. *Am. J. Phys.* **71**, 233–242. (doi:10.1119/1.1522698)
8. Gutiérrez-Vega JC, Iturbe-Castillo MD, Ramirez GA, Tepichin E, Rodriguez-Dagnino RM, Chavéz-Cerda S, New GHC. 2001 Experimental demonstration of optical Mathieu beams. *Opt. Commun.* **195**, 35–40. (doi:10.1016/S0030-4018(01)01319-0)
9. Ruby L. 1995 Applications of the Mathieu equation. *Am. J. Phys.* **64**, 39–44. (doi:10.1119/1.18290)
10. Chen HS, Mei CC. 1971 Scattering and radiation of gravity waves by an elliptical cylinder. Technical report no. 140. Parsons Laboratory, Department of Civil engineering, MIT, **17**, 61–71.
11. Chen HS, Mei CC. 1973 Wave forces on a stationary platform of elliptical shape. *J. Ship Res.* **17**, 61–71.
12. Williams AN. 1985 Wave diffraction by elliptical breakwaters in shallow water. *Ocean Eng.* **12**, 25–43. (doi:10.1016/0029-8018(85)90009-5)
13. Williams AN, Darwiche MK. 1988 Three-dimensional wave scattering by elliptical breakwaters. *Ocean Eng.* **15**, 103–118. (doi:10.1016/0029-8018(88)90022-4)
14. Chatjigeorgiou IK, Mavrakos SA. 2009 Hydrodynamic diffraction by multiple elliptical cylinders. In *Proc. 14th Int. Workshop on Water Waves and Floating Bodies, Zelonogorosk, Russia, 19–22 April*, pp. 38–41. See http://www.iwwwfb.org/Workshops/24.htm.
15. Chatjigeorgiou IK, Mavrakos SA. 2010 An analytical approach for the solution of the hydrodynamic diffraction by arrays of elliptical cylinders. *Appl. Ocean Res.* **32**, 242–251. (doi:10.1016/j.apor.2009.11.004)
16. Carr JH, Stelzriede ME. 1951 Diffraction of water waves by breakwaters. In *Proc. of the NBS Semicentennial Symp. on Gravity Waves, Gaithersburg, MD, 18–20 June*, pp. 109–125. Gaithersburg, MD: Natural Bureau of Standards (National Institute of Standards and Technology).
17. Michele S, Sammarco P, d'Errico M, Renzi E, Abdolali A, Bellotti G, Dias F. 2015 Flap gate farm: from Venice lagoon defense to resonating wave energy production. Part 2: synchronous response to incident waves in open sea. *Appl. Ocean Res.* **52**, 43–61. (doi:10.1016/j.apor.2015.05.002)
18. Michele S, Sammarco P, d'Errico M. 2016 The optimal design of a flap gate array in front of a straight vertical wall: resonance of the natural modes and enhancement of the exciting torque. *Ocean Eng.* **118**, 152–164. (doi:10.1016/j.oceaneng.2016.04.002)
19. Sammarco P, Michele S, d'Errico M. 2013 Flap gate farm: from Venice lagoon defense to resonating wave energy production. Part 1: natural modes. *Appl. Ocean Res.* **43**, 206–213. (doi:10.1016/j.apor.2013.10.001)
20. Mei CC, Sammarco P, Chan ES, Procaccini C. 1994 Subharmonic resonance of proposed storm gates for Venice lagoon. *Proc. R. Soc. Lond. A* **444**, 257–265. (doi:10.1098/rspa.1994.0016)
21. Sammarco P, Tran HH, Mei CC. 1997 Subharmonic resonance of Venice gates in waves. Part 1. Evolution equation and uniform incident waves. *J. Fluid Mech.* **349**, 295–325. (doi:10.1017/S0022112097006848)
22. Sammarco P, Tran HH, Gottlieb O, Mei CC. 1997 Subharmonic resonance of Venice gates in waves. Part 2. Sinusoidally modulated incident waves. *J. Fluid Mech.* **349**, 295–325. (doi:10.1017/S0022112097006836)

23. Newman JN 1976. The interaction of stationary vessels with regular waves. In *Proc. 11th Symp. Naval Hydrodynamics, London, UK, 28 March–2 April*, pp. 491–502. London, UK: Mechanical Engineering Publications Ltd.
24. Mei CC, Stiassnie M, Yue DKP. 2005 *Theory and applications of ocean surface waves*. Singapore: World Scientific.
25. Goda Y. 2000 *Random seas and design of maritime structures*. Singapore: World Scientific.
26. Martin PA, Rizzo FJ. 1989 On boundary integral equations for crack problems. *Proc. R. Soc. Lond. A* **421**, 341–355. (doi:10.1098/rspa.1989.0014)
27. Linton CM, McIver P. 2001 *Mathematical techniques for wave/structure interactions*. London, UK: Chapman & Hall/CRC.
28. Mei CC. 1997 *Mathematical analysis in engineering*. Cambridge, UK: Cambridge University Press.
29. Gradshteyn IS, Ryzhik IM. 2007 *Tables of integrals series and products*. New York, NY: Academic Press.
30. Martin PA. 1991 End-point behaviour of solutions to hypersingular integral equations. *Proc. R. Soc. Lond. A* **432**, 301–320. (doi:10.1098/rspa.1991.0019)
31. Gutiérrez-Vega JC. 2000 Formal analysis of the propagation of invariant optical fields in elliptic coordinates. PhD thesis, INAOE, México.